Journal of Alloys and Compounds 843 (2020) 156007

Contents lists available at ScienceDirect

Journal of Alloys and Compounds

journal homepage: http://www.elsevier.com/locate/jalcom

Saline slag waste as an aluminum source for the synthesis of Zn–Al–Fe–Ti layered double-hydroxides as catalysts for the photodegradation of emerging contaminants

L. Santamaría [a], M.A. Vicente [b], S.A. Korili [a], A. Gil [a, *]

[a] INAMAT-Departamento de Ciencias, Edificio de los Acebos, Universidad Pública de Navarra, Campus de Arrosadía, 31006, Pamplona, Spain
[b] GIR-QUESCAT, Departamento de Química Inorgánica – Universidad de Salamanca, 37008, Salamanca, Spain

ARTICLE INFO

Article history:
Received 21 January 2020
Received in revised form
29 May 2020
Accepted 7 June 2020
Available online 15 June 2020

Keywords:
aluminum industrial waste
Photocatalyst
Adsorption
Diclofenac
Salicylic acid
Hydrotalcite
Layered double hydroxides
Saline slags

ABSTRACT

In this work, aluminum extracted from saline slag waste is valorized to create a layered double-hydroxide series containing zinc and various proportions of aluminum/titanium. Materials were synthesized by the co-precipitation method with an Me^{2+}/Me^{3+} molar ratio of 3:1 and tested for the removal of diclofenac and salicylic acid from water under UV radiation. The incorporation of 5 wt% iron by wet impregnation is evaluated. In addition, another series of zinc, aluminum/iron materials with and without 5 wt% impregnated titanium are tested as catalysts for comparison. Structural characterization and comparison of the two series was performed by powder X-ray diffraction (PXRD), nitrogen adsorption at 77 K, scanning electron microscopy (SEM), X-ray photoelectron spectroscopy (XPS) and temperature-programmed reduction (TPR) measurements. The uncalcinated samples had a typical hydrotalcite structure with a high crystallinity; the presence of ZnO, $ZnFe_2O_4$ or Fe_3O_4 was found after calcination. The specific surface areas of the dried samples ranged from 78 to 199 m^2/g, being highest for $Zn_6Al_{0.5}Ti_{1.5}$. Overall, the results showed that the ZnAlTi series were more effective catalysts than ZnAlFe for photodegradation of the emerging contaminants diclofenac and salicylic acid, under UV light at 298 K, considering two concentrations of the organic molecules (5 and 50 μmol/dm^3).

© 2020 Elsevier B.V. All rights reserved.

1. Introduction

Recent progress in analytical methods and scientific instrumentation [1,2] in the field of emerging contaminants show that a reliable approach to solving current water pollution problems should be an environmental priority. In this context, one of the family of materials that has received great attention lately as a possible alternative to TiO_2 is that of layered double hydroxides (LDHs), which have proven to be effective in both adsorption [3,4] and catalysis, more specifically photocatalysis [3,5–9]. LDHs, which are also known as anionic clays, are synthetic minerals with a structure similar to that of brucite ($Mg(OH)_2$). Substitution of part of the Me^{2+} ions by Me^{3+} generates a positive charge in the layers, which is compensated by the inclusion of anions to give the general formula $[Me^{2+}_{1-x}Me^{3+}_{x}(OH)_2]^{x+}(A^{n-})_{x/n}\bullet mH_2O$, where A is the anion intercalated in between the layers (usually CO_3^{2-}). Their octahedral framework confers LDHs with several characteristics that are very useful for photocatalysis. For instance, Me^{2+} and Me^{3+} present in the structure of LDHs are distributed in a uniform manner in the hydroxide layers, thus meaning that the high degree of dispersion of the transition metal octahedra enables electron transfer and avoids the recombination of electrons and holes. Similarly, the surface OH^- groups of the brucite layers react with valence band holes to yield hydroxyl radicals (•OH), which have a very high oxidation potential and are considered to be an important intermediate for photo-oxidation reactions [10]. Apart from the fundamental structure, several modifications have proven to be effective for photodegradation. Thus, metal ion doping can give LDHs the properties of doped semiconductors [11], and the combination with TiO_2 may enhance performance as a result of the surface OH^- groups [12,13]. LDHs contain two or more different metal ions and the proportion between these metals can be controlled, as in doped semiconductors, where a higher valent cation acts as dopant. The presence of different transition metal ions enables LDHs to exhibit a broad spectrum of photocatalysis properties. Thus, the combination of metals such as CoCr, CuCr, ZnCr, ZnFe, ZnTi, MgCr, MgFe and NiFe

* Corresponding author.
E-mail address: andoni@unavarra.es (A. Gil).

https://doi.org/10.1016/j.jallcom.2020.156007
0925-8388/© 2020 Elsevier B.V. All rights reserved.

leads to a photoresponse in these materials. The interlayer space also plays an important role in improving the photocatalytic performance as this space facilitates the reaction between the photogenerated charge carriers and the reactant molecules. Finally, as photodegradation is a surface phenomenon, a previous adsorption process is advantageous to make the material more efficient [6,14]. LDHs can take up species by either surface adsorption or by the "memory effect", in other words reconstruction of the hydrotalcite structure when suspended in water, although this structure is lost after calcination. This uncommon layered structure, combined with their straightforward synthesis, low cost and compositional flexibility, has made LDHs one of the most promising alternatives to TiO_2 as photocatalysts in advanced oxidation processes.

The environmental problems surrounding the disposal of industrial waste, such as the leaching of hazardous heavy metals [15] or the emission of particulate material [16], suggest that the valorization of waste materials is the most appropriate method to overcome these problems [17]. Only a limited number of methods, including incineration, storage in landfills and security tanks, stabilization, amongst others, are available for the treatment of hazardous wastes. The best method, however, is valorization (either total or partial) of its components. If these possibilities are not applicable, the only option is storage in security tanks. In the present work, a further step forward is proposed as the aluminum present in the catalyst is obtained from a valorization process developed by our group [4,18]. Saline slags are generated during the secondary aluminum processing, i.e. the recycling of aluminum. Their average composition includes mainly metallic aluminum, several oxides and flux brines as principal components, with the content of non-metallic products varying depending on the nature of the material recycled [19,20]. As the difference in composition makes it difficult to propose a standard recovery method, waste is currently stored in controlled landfills. In this context, a few successful valorization strategies have been described previously. For example, Cocheci et al. [21] extracted zinc from zinc ash generated during the hot-dip galvanizing process to form ZnAl–CO_3-LDH, and Galindo et al. [22] synthesized MgAl–CO_3-LDH using aluminum extracted from the waste generated in the tertiary aluminum industry. Similarly, both Murayama et al. [23], who synthesized MgAl–CO_3-LDH from aluminum dross, and Kuwahara et al. [24], who used blast furnace slags generated in the iron making process to form CaAl–CO_3-LDH, tested their adsorption properties towards arsenic and phosphate, respectively, and Das et al. [25] reported the synthesis of LDH containing Mg, Al and Ti from titanium-rich bauxite applied to the removal of fluoride and chromium (IV). All these studies rely upon acid leaching to perform the extractions. However, as LDH synthesis has to be carried out at a constant basic pH of between 9 and 10, a more cost-effective approach may involve basic extraction of the aluminum. To the best of our knowledge, the photodegradation ability of such *valorized* LDHs has never been tested as no further uses, other than for adsorption, have been found.

Salicylic acid and diclofenac were chosen as emergent contaminants as they are the most widely consumed non-steroidal anti-inflammatory drugs (NSAIDs). The high toxicity of diclofenac, even at low concentrations, the low capacity of wastewater treatment plants to retain it [26], and the detection of both salicylic acid and diclofenac in drinking water are their main causes of concern in this regard [27,28].

In this work, two series of Zn–Al–CO_3 LDHs prepared using aluminum obtained from the basic extraction of saline slags have been tested for the photodegradation of diclofenac and salicylic acid. Several different proportions of Fe^{3+} and $Ti^{3+/4+}$ were used to dope (in the structure) or impregnate (on the surface) the LDHs. One series consisted of Zn–AlFe–CO_3 LDH with various Al/Fe ratios as Me^{3+} and impregnated with 5 wt% titanium (labelled as 5Ti/), and the other series comprised Zn–AlTi–CO_3 LDH with Al/Ti various ratios and impregnated with 5 wt% iron (labelled as 5Fe/).

2. Experimental procedure

2.1. Materials

The materials used to synthesize hydrotalcites were $Zn(NO_3)_2 \bullet 6H_2O$ (≥98%, Sigma-Aldrich), Na_2CO_3 (≥99.99%, Sigma-Aldrich), $TiCl_3$ (≥12%, Sigma-Aldrich), $Ti[OCH(CH_3)_2]_4$ (>97%, Sigma Aldrich), $Fe(NO_3)_3 \bullet 9H_2O$ (Riedel-deHaën, >96%), and NaOH (Panreac) for pH adjustment and aluminum extraction. Salicylic acid (2-hydroxybenzoic acid, 2-$(HO)C_6H_4COOH$, ≥ 99.99%, Sigma-Aldrich) and diclofenac sodium salt (2-[(2,6-dichlorophenyl) amino]benzeneacetic acid sodium salt, $C_{14}H_{10}Cl_2NNaO_2$, Sigma-Aldrich) were also used as received.

2.2. Synthesis of hydrotalcite-like compounds

The material used in the present study was an aluminum saline slag previously treated with hot water in order to separate the soluble salts. The main characteristics of this slag waste were reported previously [29]. This material was submitted to aluminum chemical extraction, which was carried out using 2 mol/dm^3 aqueous solutions of NaOH, for 2 h under reflux conditions, the extracted aluminum subsequently being used to synthesize the hydrotalcites [18]. Layered double-hydroxides containing $Zn_6(AlFe)_2$ at various Al/Fe proportions and with a Zn^{2+}/Me^{3+} molar ratio of 3:1 were prepared at a constant pH of 10 using the co-precipitation method [18]. For the synthesis, 200 cm^3 of a 0.75 mol/dm^3 solution of Zn^{2+} and 0.25 mol/dm^3 solution of $(Al^{3+} + Fe^{3+})$ were added dropwise to a stirred solution of Na_2CO_3 (0.2 mol/dm^3). The resulting solid materials were separated by filtration and washed with hot water to remove unreacted substances. The cakes obtained were dried at 333 K for 16 h, calcinated at 673 K for 4 h to remove the anions from the interlayer, and then impregnated with 5 wt% titanium (IV) isopropoxide. Another series containing $Zn_6(AlTi)_2$ with various Al/Ti proportions and using $TiCl_3$ as titanium source was also synthesized following the same procedure and impregnated with 5 wt% iron. Finally, all materials were calcinated at 673 K for 4 h.

2.3. Characterization of the catalysts

The texture of the samples (0.4 g), previously degassed at 423 K for 24 h at a pressure of less than 0.1 Pa, was analyzed by low temperature nitrogen (Praxair, 99.999%) adsorption at 77 K using a Micromeritics ASAP 2020 Plus adsorption analyzer. The amount of nitrogen adsorbed at a relative pressure of 0.98 was used to estimate the total pore volume (V_p) and the surface area of the samples was calculated using the Brunauer-Emmer-Teller (BET) method. The crystalline phases present in the samples were identified by powder X-ray diffraction (PXRD) and patterns were obtained using a Siemens D-5000 X-ray diffractometer with Ni-filtered Cu Kα radiation ($\lambda = 0.1548$ nm). The working conditions were 30 mA, 40 kV in a 2θ range from 5 to 70° and a scanning rate of 2° (2θ)/min. Thermogravimetric measurements were performed using a Hi-Res TGA2950 apparatus (TA-Instruments), heating from room temperature up to 1173 K at a rate of 10 K/min under an air atmosphere (60 cm^3/min). Scanning electron microscopy (SEM) was used to analyze the morphology of the samples (Phenom Pro X, Paralab). X-ray photoelectron spectra (XPS) were recorded using a SPECS Phoibos 150 1DDLD spectrometer equipped with an Al Kα source (1486.7 eV). Temperature-programmed reduction (TPR) studies

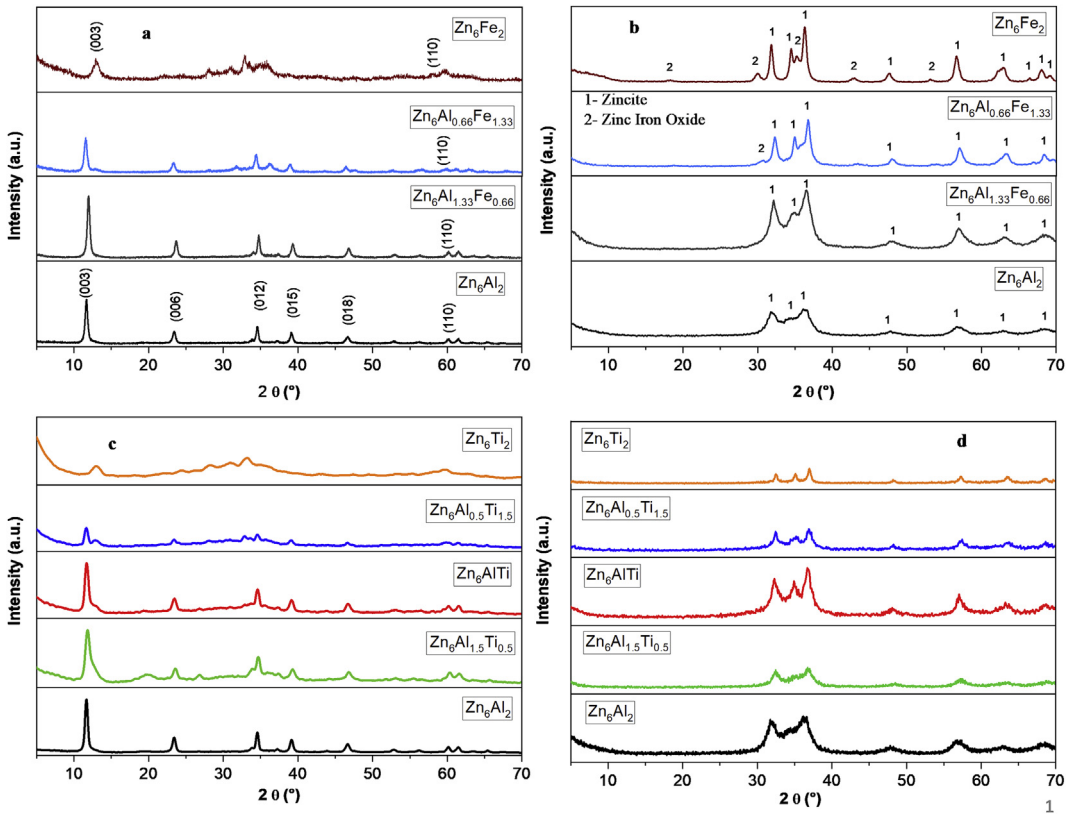

Fig. 1. Powder X-ray diffraction patterns for non-calcinated samples (a: Zn–Al–Fe; c: Zn–Al–Ti) and after treatment at 673 K (b: Zn–Al–Fe; d: Zn–Al–Ti).

Table 1
Basal spacing, and *c* and *a* parameters for the non-calcinated ZnAlFe-LDH and ZnAlTi-LDH samples.

Sample	$d_{(003)}$	***c*** (nm)	$d_{(110)}$	***a*** (nm)
Zn_6Al_2	0.761	2.278	0.153	0.307
$Zn_6Al_{1.33}Fe_{0.66}$	0.739	2.233	0.154	0.307
$Zn_6Al_{0.66}Fe_{1.33}$	0.766	2.289	0.154	0.307
Zn_6Fe_2	0.688	2.063	0.158	0.316
$Zn_6Al_{1.5}Ti_{0.5}$	0.752	2.253	0.153	0.306
Zn_6AlTi	0.757	2.275	0.153	0.307
$Zn_6Al_{0.5}Ti_{1.5}$	0.761	2.281	0.153	0.307
Zn_6Ti_2	0.686	2.059	0.155	0.310

were carried out using a Micromeritics TPR/TPD 2900 instrument under a total flow of 30 cm^3/min of carrier gas (5% H_2 in Ar) and a heating rate of 10 K/min up to 1050 K. The samples (20 mg) were first pretreated with N_2 (Praxair, 99.999%) at a heating rate of 10 K/min up to 473 K for 120 min. Water and other compounds that might be formed during the metal reduction and precursor decomposition were retained by a cold trap (isopropyl alcohol/liquid nitrogen), thus avoiding possible interferences with the measured signal.

2.4. Degradation procedure

The photodegradation of salicylic acid and diclofenac under ultraviolet (UV) radiation was analyzed using the calcinated

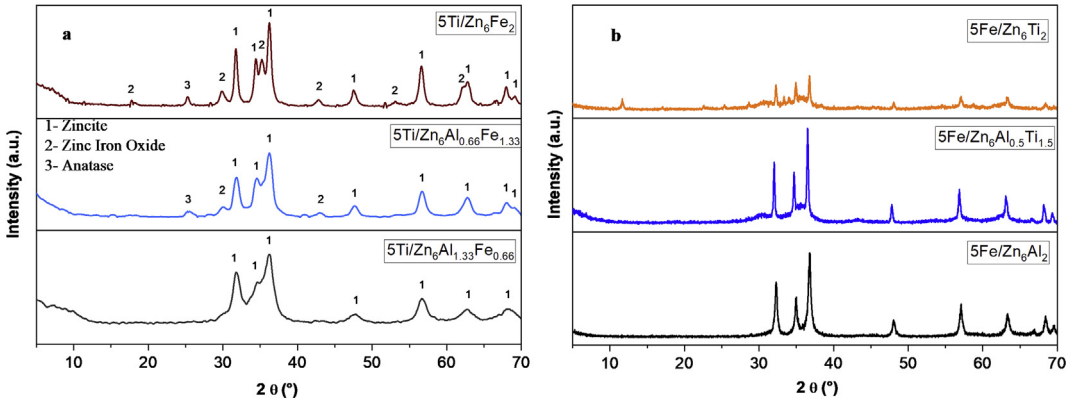

Fig. 2. Powder X-ray diffraction patterns for (a) ZnAlFe-LDH series impregnated with 5 wt% titanium, and (b) ZnAlTi-LDH series impregnated with 5 wt% iron.

samples as catalysts. The process was carried out in a photon cabinet containing a 1 dm^3 PhotoLAB Batch-L reactor (MPDS-Basis system from UV-Consulting Peschl) with a 150 W medium-pressure TQ 150Z1 Hg lamp (continuous spectrum, with mean peaks at 366 and 313 nm) enclosed in a cooling jacket to maintain a constant temperature of 298 K. A 700 cm^3 solution of diclofenac at a concentration of either 5 or 50 μmol/dm^3 was mixed in the reactor with the catalyst and stirred at 700 rpm and a concentration of 1.0 $g_{catalyst}/dm^3$ under UV radiation. Samples were taken every 15 min, filtered and the drug concentration measured using a UV−vis spectrometer (Jasco V-730) at its maximum adsorption wavelength (276 nm). The same procedure and concentrations were used for salicylic acid (λ_{max} 297 nm). Adsorption tests, without irradiation, were carried out for every experiment, and photolysis tests, in the absence of a catalyst, were also performed.

3. Results and discussion

3.1. Characterization of hydrotalcites

The X-ray diffraction patterns of the non-calcinated samples from series ZnAlFe and ZnAlTi are shown in Fig. 1a and c. These aluminum-containing samples clearly exhibit a double layered hydroxide type structure, which is less defined in Zn_6Fe_2 and Zn_6Ti_2. All samples have a well-defined peak at $2\theta \approx 12^\circ$ that matches the (003) reflection and an interlayer distance characteristic of hydrotalcite-like materials, in accordance with the results reported by other authors [12,13,30−32]. If a 3R symmetry is assumed [33], the cell parameters can be calculated applying the Bragg equation [34] using the values for the (003), (006) and (110) reflections to give $c = 3\ [1/2\ (d_{003} + 2d_{006})]$ and $a = 2d_{110}$. The values for c and a (see Table 1) show an opposite trend, with the average metal-metal distance increasing as the interlayer distance decreases. These results are in accordance with the radii of the cations incorporated into the LDH as, for example, the ionic radius of Fe^{3+} is larger than that of Al^{3+} [35]. The LDH structure disappears after calcination of the samples at 673 K, leading to a zincite pattern (ZnO phase) as well as to the possible presence of the zinc aluminate spinel $ZnAl_2O_4$ (see Fig. 1b and d). Cheng et al. [36] found that the layered structure of ZnAl hydrotalcites was preserved after thermal treatment at 423 and 473 K, although the crystallinity was lowered given the broadening of the lines and decrease in their intensities. The LDH phase decreased and was replaced by ZnO and $ZnAl_2O_4$ spinel phases as the calcination temperature increased. A similar loss of crystallinity and the appearance of ZnO at 473 K were described previously by dos Reis et al. [37]. The preparation and characterization of various ZnAl hydrotalcites have also been reported by Carriazo el al [31]. After calcination at 773 K, these authors found collapse of the layered structure and new diffraction lines related to several metal oxides, including ZnO and the $ZnAl_2O_4$ spinel. The crystallinity of these oxides increased at calcination temperatures higher than 773 K, as suggested by the higher intensity and sharpness of the diffraction lines. A similar behavior was also found by Hadnadjev-Kostic et al. [38]. As more iron is incorporated into the samples, the peaks become more defined and zinc iron oxide ($ZnFe_2O_4$) appears in the diffractogram [39]. In the case of the samples synthesized in the presence of titanium, no diffraction peaks corresponding to TiO_2, $ZnTiO_3$ or Zn_2TiO_4 phases were observed [38,40−43], thus suggesting a possible high dispersion of the oxides or a low crystallinity. These phases were found by Seftel et al. [44] after thermal treatment at 873 K. Impregnation of the samples with 5 wt% titanium did not significantly change their structure, although low intensity anatase peaks were observed for $5Ti/Zn_6Al_{0.66}Fe_{1.33}$ and $5Ti/Zn_6Fe_2$ (Fig. 2a). Similarly, impregnation of the ZnAlTi series with 5 wt% iron (patterns shown in Fig. 2b) also led to the zincite structure. The addition of iron cannot be observed in the patterns, although the peaks

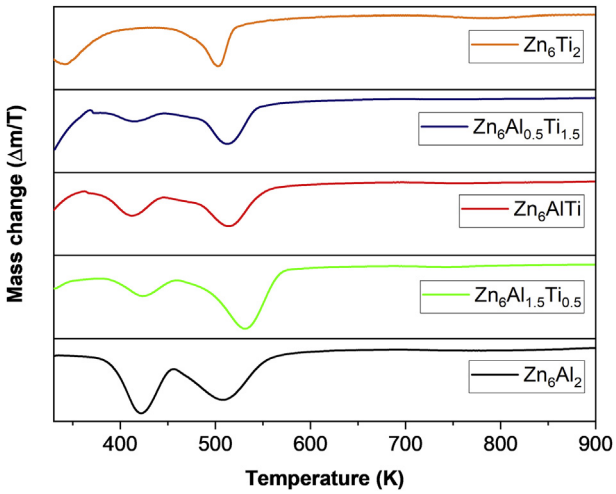

Fig. 4. DGT curves for the ZnAlTi-LDH materials.

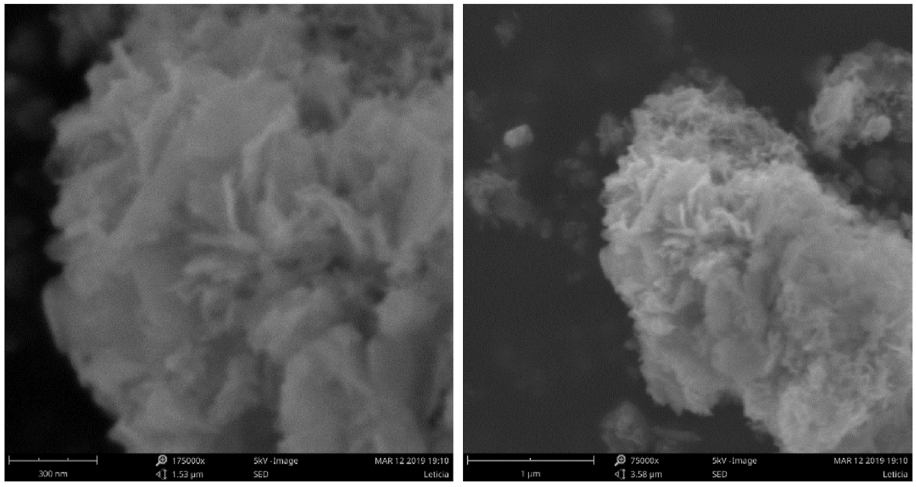

Fig. 3. SEM micrographs of $Zn_6Al_{1.33}Fe_{0.66}$.

formed are sharper and better defined after impregnation.

Although the PXRD patterns display a structural change in the samples as a result of the calcination process, the SEM images of sample $Zn_6Al_{1.33}Fe_{0.66}$ after calcination clearly show differentiated rose petal-like shapes (Fig. 3). The layered structure of the samples is still preserved, as reported previously [45,46].

Thermogravimetric analysis showed the presence of five mass-loss steps (see Fig. 4). The first two mass losses, between 298 and 423 K, are related to the loss of water (adsorbed on the surface and located in the interlayer). The third step, centered at around 523 K, is related to dehydroxylation and decarbonation processes, whereas the following two steps, between 673 and 1123 K, have low intensity and may be related to further decomposition of the mixed oxides.

The adsorption-desorption isotherms for the non-calcinated, calcinated, Ti-impregnated ZnAlFe-LDH and Fe-impregnated ZnAlTi-LDH are presented in Fig. S1. All N_2 adsorption isotherms are type II in the IUPAC classification, where N_2 adsorption does not reach a plateau at high relative pressures. In all cases, the desorption branch leads to an H3 hysteresis loop, which may indicate small, slit-shaped pores. The BET surface areas and total pore volumes are shown in Table 2. For uncalcinated Zn_6Me_2 samples, Zn_6Ti_2 had the largest BET specific surface area (184 m^2/g), while Zn_6Al_2 had the lowest (78 m^2/g). Calcination at 673 K caused a marked decrease in the BET surface area of some samples, with the initial value decreasing by between 29% ($Zn_6Al_{0.66}Fe_{1.33}$) and 57% (Zn_6Fe_2). The BET surface areas for $Zn_6Al_{1.33}Fe_{0.66}$ and Zn_6Al_2 were not modified by the calcination process. Impregnation of the samples with 5 wt% titanium or iron did not cause major changes in the BET surface areas of the samples, with a small decrease in 5Ti/$Zn_6Al_{1.33}Fe_{0.66}$, from 112 to 109 m^2/g, and small increases in the other two samples (Zn_6Fe_2 from 53 to 55 m^2/g and $Zn_6Al_{0.66}Fe_{1.33}$ from 72 to 84 m^2/g). In the case of the ZnAlTi-LDH series, all BET surface areas were similar, with 5Fe/Zn_6Ti_2 having the smallest value (71 m^2/g).

The H_2-TPR profiles obtained for the calcinated ZnAlTi-LDH series are shown in Fig. 5a. Before iron impregnation, the Zn_6Al_2 sample did not give any strong signal, with only a small peak at around 850 K that could be related to the reduction of Zn^{2+} to Zn^0 as a result of the presence of amorphous ZnO and $ZnAl_2O_4$ [47]. When iron is added, two distinctive peaks, which are assigned to different Fe^{3+} reduction steps, appear at 690 and 850 K. When pure iron oxide is considered, Fe_2O_3 is reduced to Fe_3O_4 at around 850 K and a second reduction peak, which combines the reduction of Fe_3O_4 to FeO and to Fe^0, appears at around 1000 K [48]. In the case of $ZnFe_2O_4$, a direct reduction to Fe_3O_4 and then to FeO and Fe has been suggested, with the presence of three reduction peaks [49]. $ZnFe_2O_4$ is more prone to be reduced as the presence of the semiconductor ZnO promotes the reduction of metal oxides [49,50], as also reported in the case of Ni-Zn-Al [51] and Fe–Zn–Al [39] hydrotalcites. When iron is impregnated on $Zn_6Al_{0.5}Ti_{1.5}$ and Zn_6Ti_2, these peaks are not so easily observed and a wider peak seems to overlap several reduction stages, in other words reduction of Fe_3O_4 to FeO occurs at a lower temperature, probably due to the smaller particle size, lower cristallinity and, consequently, greater instability of the samples [52]. The H_2-TPR profiles for the ZnAlFe-LDH series are shown in Fig. 5b. H_2 consumption increases with iron content in the LDH, with the Zn_6Fe_2 signal having almost double the intensity of that for $Zn_6Al_{1.33}Fe_{0.66}$. The addition of titanium onto the surface causes minor changes in the $Zn_6Al_{1.33}Fe_{0.66}$ and $Zn_6Al_{0.66}Fe_{1.33}$ H_2 consumption profiles, with the $ZnFe_2O_4$ reduction peak being less-well resolved, possibly because H_2 has greater difficulty in accessing $ZnFe_2O_4$ once the titanium has been impregnated. In Zn_6Fe_2, however, the addition of titanium lowers the temperature of Fe_3O_4 reduction from 959 to 750 K, and that of $ZnFe_2O_4$ from 750 to 650 K. In the case of titanium oxide, a partial reduction of Ti^{4+} to Ti^{3+} could occur in the temperature range studied; this process has been reported to occur at 838 K [53]. As described above, other reduction processes also occur at this temperature, therefore it was not possible to differentiate which

Table 2
BET specific surface areas and total pore volumes for the ZnAlFe and ZnAlTi-LDH samples.

		Sample	S_{BET} (m^2/g)	V_p (cm^3/g)
ZnAlFe–LDH series	Non-calcined samples	Zn_6Al_2	78	0.384
		$Zn_6Al_{1.33}Fe_{0.66}$	114	0.558
		$Zn_6Al_{0.66}Fe_{1.33}$	102	0.537
		Zn_6Fe_2	124	0.497
	Calcined samples	Zn_6Al_2	77	0.348
		$Zn_6Al_{1.33}Fe_{0.66}$	112	0.640
		$Zn_6Al_{0.66}Fe_{1.33}$	72	0.307
		Zn_6Fe_2	53	0.316
		5Ti/Zn_6Al_2	91	0.361
		5Ti/$Zn_6Al_{1.33}Fe_{0.66}$	109	0.494
		5Ti/$Zn_6Al_{0.66}Fe_{1.33}$	84	0.330
		5Ti/Zn_6Fe_2	55	0.291
ZnAlTi–LDH series	Non-calcined samples	Zn_6Al_2	78	0.384
		$Zn_6Al_{1.5}Ti_{0.5}$	152	0.640
		Zn_6AlTi	152	0.522
		$Zn_6Al_{0.5}Ti_{1.5}$	199	0.517
		Zn_6Ti_2	184	0.497
	Calcined samples	Zn_6Al_2	79	0.345
		$Zn_6Al_{1.5}Ti_{0.5}$	100	0.522
		Zn_6AlTi	93	0.433
		$Zn_6Al_{0.5}Ti_{1.5}$	95	0.428
		Zn_6Ti_2	95	0.375
		5Fe/Zn_6Al_2	79	0.509
		5Fe/$Zn_6Al_{1.5}Ti_{0.5}$	81	0.474
		5Fe/Zn_6AlTi	70	0.312
		5Fe/$Zn_6Al_{0.5}Fe_{1.5}$	78	0.234
		5Fe/Zn_6Ti_2	71	0.286

processes these signals correspond to.

X-ray photoelectron spectroscopy is a useful technique for investigating the surface composition and chemical states of the elements present on the solid samples. The surface concentration and proposed elemental formulae for the calcinated compounds present on the surface of the LDH can be found in Table 3. The O 1s core level spectra of the samples for the two series are shown in Fig. 6. The signal can be split into two peaks in all aluminum-containing samples. The first peak (≈530 eV) was attributed to the lattice oxygen bound to metal cations of the structure (both Zn_6Fe_2 and Zn_6Ti_2 samples have this peak exclusively), whereas the second peak is found at higher binding energy (≈531.5 eV) and can be attributed mainly to hydroxyl groups, although a small percentage of this peak is associated with organic contamination and chemisorbed water [54]. The presence of these hydroxyl groups can benefit the photocatalytic process as they help to create hydroxyl radicals (•OH) [53]. In all cases, the addition of 5 wt % of either Fe or Ti favors the increase of oxygen bound to metal cations as Ti is added as TiO_2 and Fe as Fe_3O_4 (Fe^{2+} represents 33% and Fe^{3+} 66% in the three samples).

3.2. Degradation and adsorption experiments

Photolysis experiments were performed with diclofenac and salicylic acid, resulting in degradation percentages of 6% and 0%, respectively. In the case of the adsorption experiments, the results obtained indicate that this process is important in some cases, thus meaning that each particular case should be discussed individually to explain the photodegradation results.

3.2.1. ZnAlTi-LDH series with and without iron

The hydrotalcites with the composition ZnAlTi showed a higher ability to degrade diclofenac and salicylic acid than their ZnAlFe counterparts. The change in contaminant concentration in relation to the initial concentration when using 5 μM solutions of diclofenac and salicylic acid and 1 g/dm^3 of catalyst are plotted in Fig. 7a and c, respectively. Zn_6Al_2 is much more effective at removing both drugs than the other two samples (Zn_6Ti_2 and $Zn_6Al_{0.5}Ti_{1.5}$). In order to be able to discern the contribution of the catalytic process, the adsorption capacity of these materials was also investigated under the same experimental conditions. These results are included in Table 4. From the diclofenac results, it can be seen that the adsorption capacity decreases as the amount of Ti in the samples increases. In the most favorable case (Zn_6Al_2), and for a concentration of 5 μmol/dm^3, 93% is adsorbed and in the worst case, adsorption was null (Zn_6Ti_2). At a higher concentration (50 μmol/dm^3) the percentage adsorbed is lower. Under the conditions of photodegradation, no differences were observed with respect to the adsorption tests when the initial concentration was 5 μmol/dm^3, with the quantity of diclofenac eliminated increasing if the concentration of 50 μmol/dm^3 is considered. According to previous studies from our research group, these series of hydrotalcites adsorb less salicylic acid than diclofenac, and thus, in the case of salicylic acid, there is a clear difference between the amounts adsorbed and photodegraded, although no differences are observed between the two concentrations (5 and 50 μmol/dm^3). The difference between these materials is the Ti content and the degree of crystallinity/laminar structure. Upon increasing the Ti content and decreasing the degree of crystallinity/layered structure, the adsorption capacity of these materials is also decreased. In this case, a well-defined LDH structure favors the adsorption of these contaminants.

When 5 wt% iron was incorporated by impregnation into the surface of the materials (see Fig. 7b for diclofenac and 7d for salicylic acid), the adsorption results for the two molecules using 5Fe/Zn_6Al_2 are practically the same as those obtained without the presence of impregnated Fe. In the case of 5Fe/$Zn_6Al_{0.5}Ti_{1.5}$ and 5Fe/Zn_6Ti_2, although the samples still had a percentage removal by adsorption of less than 10%, their degradation performance improved significantly, with removal percentages of more than 80%. The addition of 5 wt% impregnated iron has previously been proven to improve salicylic acid degradation [52] by improving the characteristic electron-hole recombination of titanium. It has been

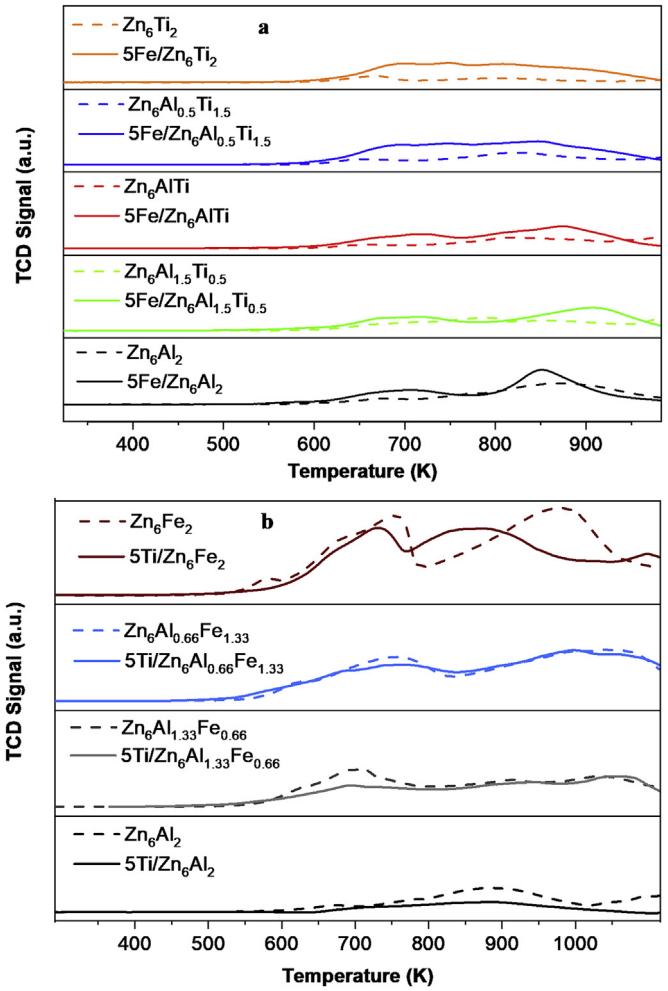

Fig. 5. H_2-TPR profile of (a) ZnAlTi-LDH and (b) ZnAlFe-LDH.

Table 3
Surface concentration (% atomic) and proposed elemental formula of the calcinated compounds on the surface of the LDH.

	Zn	Al	O	Ti	Fe	Proposed formula
Zn_6Al_2	25.6	10.4	55.9	–	–	$Zn_6Al_{2.4}$
$Zn_6Al_{1.5}Ti_{0.5}$	25	8.6	56	1.5	–	$Zn_6Al_{2.1}Ti_{0.4}$
Zn_6AlTi	25.8	5.2	56.5	4.4	–	$Zn_6Al_{1.2}Ti_{1.0}$
$Zn_6Al_{0.5}Ti_{1.5}$	26.8	3.1	55.1	5.9	–	$Zn_6Al_{0.7}Ti_{1.3}$
Zn_6Ti_2	26.5	–	56.1	9	–	$Zn_6Ti_{2.0}$
5Fe/Zn_6Al_2	16.6	12.1	53.4	–	5.0	5Fe/$Zn_6Al_{4.4}$
5Fe/$Zn_6Al_{0.5}Ti_{1.5}$	18.5	3.9	52.4	4.5	7.2	7.2Fe/$Zn_6Al_{1.3}Ti_{1.5}$
5Fe/Zn_6Ti_2	19.5	–	53.0	7.1	8.4	8.4Fe/$Zn_6Ti_{2.2}$
	Zn	Al	O	Fe	Ti	Proposed formula
$Zn_6Al_{1.33}Fe_{0.66}$	24.6	7.6	55.5	3.3	–	$Zn_6Al_{1.8}Fe_{0.8}$
$Zn_6Al_{0.66}Fe_{1.33}$	29.5	3.6	56	5.3	–	$Zn_6Al_{0.7}Fe_{1.1}$
Zn_6Fe_2	34.1	–	53.5	6.6	–	$Zn_6Fe_{1.2}$
5Ti/$Zn_6Al_{1.33}Fe_{0.66}$	21.0	7.0	54.2	2.7	3.3	3.3Ti/$Zn_6Al_2Fe_{0.77}$

reported that the induced photoexcitation can cause charge mobility and form photoactive defects in the case of LDH materials [30,55], and that the number of photoinduced centers could depend on the Me^{2+}/Me^{3+} ratio. Ni et al. [12] and Shao et al. [30] found high photocatalytic performances for the degradation of Rhodamine B and Methylene Blue on ZnTi-LDH materials synthesized with a 3:1 M ratio. The presence of Fe^{3+} ions also played an important role in the degradation of phenol [11] and azo dyes [56]. Our results show that the Fe^{3+}/Ti^{3+} system is active in the photodegradation of diclofenac and salicylic acid under UV light conditions. As such, it is possible to propose a plausible photodegradation mechanism, as shown in Fig. 8.

3.2.2. ZnAlFe-LDH series with and without titanium

Overall, this series was shown to be less effective than ZnAlTi. The change in contaminant concentration in relation to the initial concentration (50 μM) of diclofenac and salicylic acid in the presence of 1 g/dm^3 of catalyst is shown in Fig. 9a and b, respectively. As in the case of the lower concentration, Zn_6Al_2 and $Zn_6Al_{1.33}Fe_{0.66}$ are much more effective at removing both contaminants than the other two samples (Zn_6Fe_2 and $Zn_6Al_{0.66}Fe_{1.33}$). The adsorption capacity of these materials was also investigated under the same experimental conditions. These results are included in Table 5. The results for diclofenac show that Zn_6Al_2 and $Zn_6Al_{1.33}Fe_{0.66}$ remove the 56% and 84% of the contaminant by adsorption. Zn_6Fe_2 and $Zn_6Al_{0.66}Fe_{1.33}$ do not result in adsorption or photodegradation. The values for salicylic acid removal are 40% removal by Zn_6Al_2 and 59% by $Zn_6Al_{1.33}Fe_{0.66}$. The values for the total decrease of salicylic acid are also higher, thus leading us to believe that some photodegradation occurs. As in the case of diclofenac, salicylic acid is not adsorbed or degraded when Zn_6Fe_2 is used. The difference between these materials is the Fe content and the degree of crystallinity/layered structure. When increasing the Fe content and decreasing the degree of crystallinity/layered structure, the adsorption capacity of these materials is also decreased. When 5 wt% titanium was incorporated into the surface of the materials by impregnation (see Fig. 9a for diclofenac and 9b for salicylic acid), the adsorption results for the two molecules using this series of catalysts was found to be practically the same as those obtained without the presence of impregnated Ti. In the case of $Zn_6Al_{1.33}Fe_{0.66}$, although the addition of 5 wt% titanium prevents the contaminant from being adsorbed slightly, this is compensated by a better degradation and overall reduction of the salicylic acid concentration by 80%. Zn_6Al_2 was also impregnated with 5 wt% titanium, although this

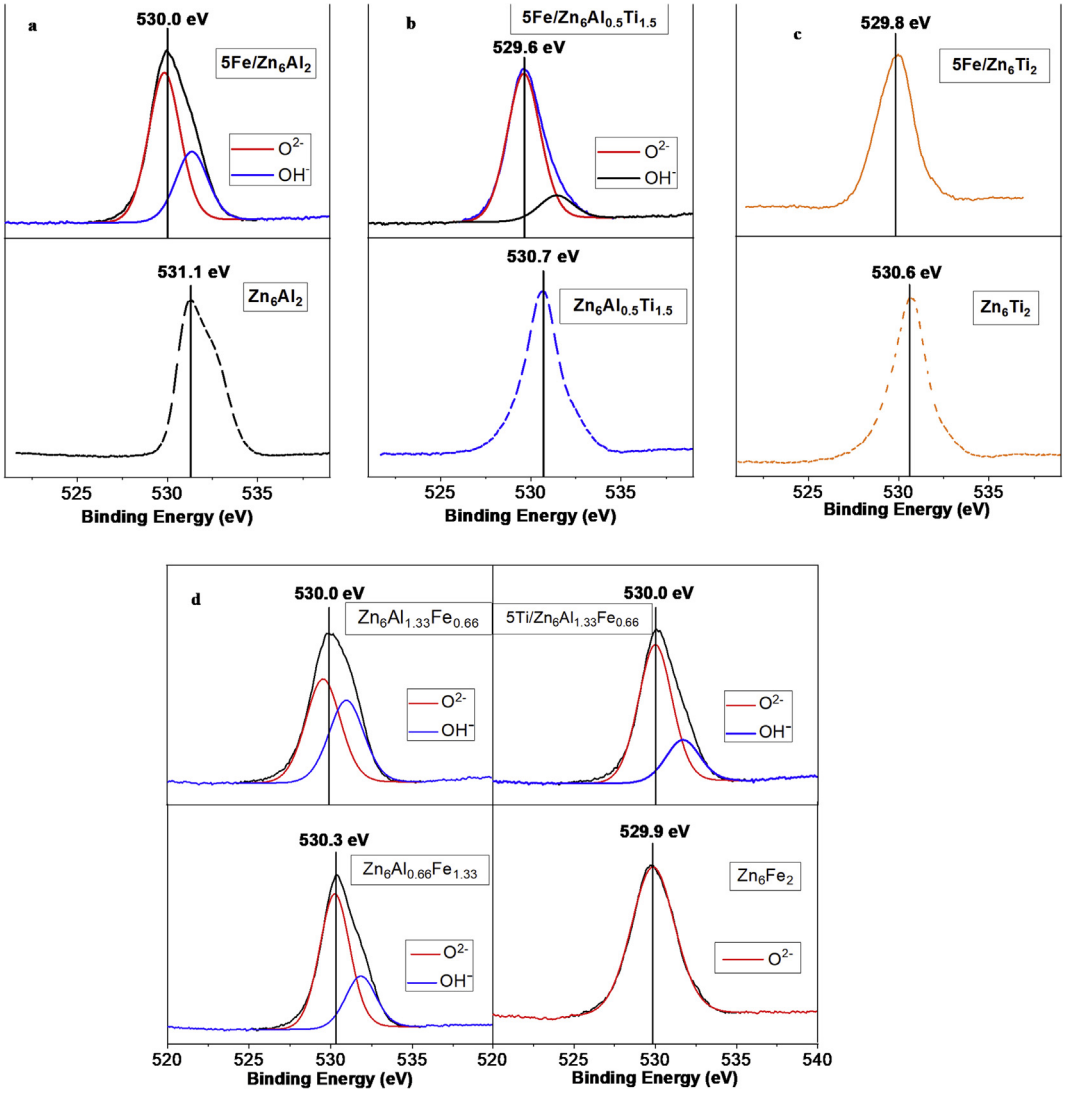

Fig. 6. XPS O 1s spectra for the ZnAlTi-LDH series (a) Zn_6Al_2, (b) $Zn_6Al_{0.5}Ti_{1.5}$, (c) Zn_6Ti_2 and (d) for the ZnAlFe-LDH series.

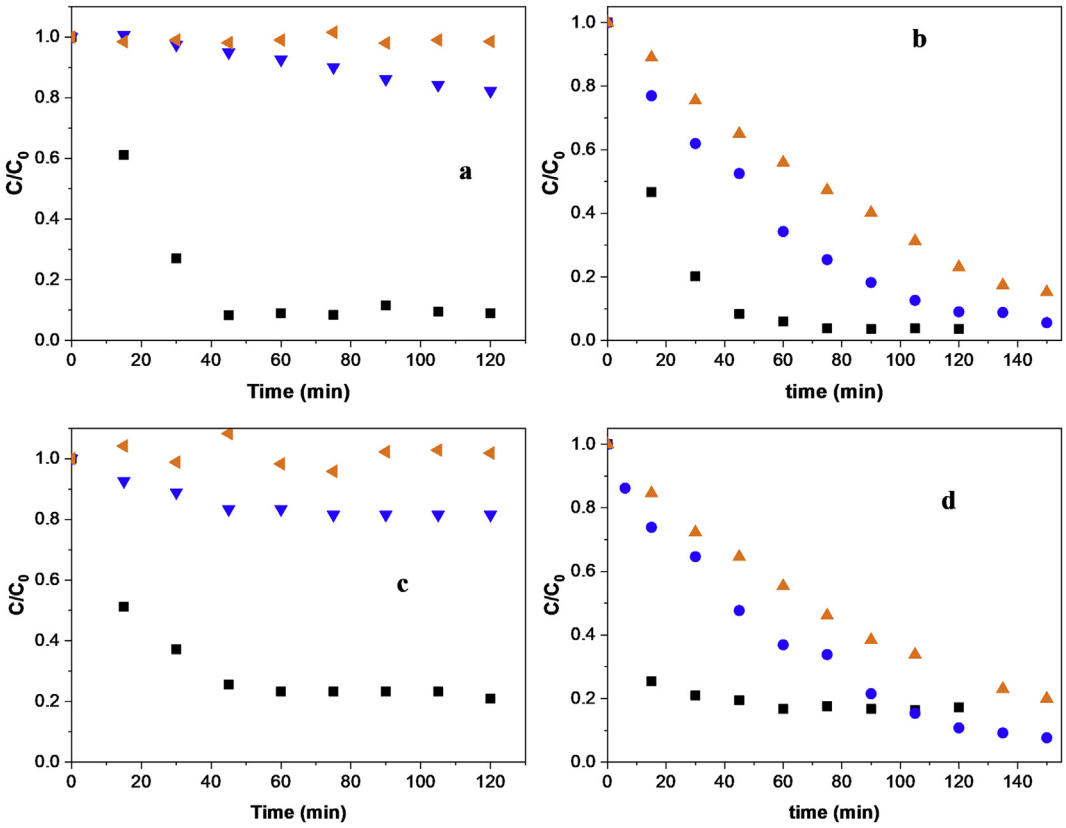

Fig. 7. Comparison of the evolution of the concentration of (a,b) diclofenac and (c,d) salicylic acid, with respect to the initial concentration, with irradiation time using (a,c) ZnAlTi-LDH and (b,d) 5Fe/ZnAlTi as catalysts (5 $\mu mol_{contaminant}/dm^3$; 1 g_{sample}/dm^3).

only decreased the overall performance. In this case, the improvement in the degradation capacity did not compensate for the decrease in adsorption, and the concentration of diclofenac was double that of Zn_6Al_2 after 60 min, thus highlighting the importance of iron in the degradation process.

The reusability of Zn_6Al_2 and $5Ti/Zn_6Al_{1.33}Fe_{0.66}$ was tested over four cycles (see Fig. 10a and b). These data were also used to investigate the kinetics of diclofenac degradation based on the Langmuir-Hinshelwood model [13]:

Table 4
Diclofenac and salicylic acid removal by adsorption and photodegradation using ZnAlTi-LDH samples as catalysts.

1 g_{sample}/dm^3, 5 $\mu mol/dm^3$	Diclofenac		Salicylic acid	
Sample	Adsorption removal (%)	Total elimination (%)	Adsorption removal (%)	Total elimination (%)
Zn_6Al_2	93	91	40	79
$Zn_6Al_{1.5}Ti_{0.5}$	70	69	31	48
Zn_6AlTi	42	49	24	49
$Zn_6Al_{0.5}Ti_{1.5}$	17	18	15	19
Zn_6Ti_2	0	0	0	0
$5Fe/Zn_6Al_2$	93	96	40	83
$5Fe/Zn_6AlTi$	7	24	8	51
$5Fe/Zn_6Al_{0.5}Ti_{1.5}$	0	94 (time:150′)	6	92 (time:150′)
$5Fe/Zn_6Ti_2$	3	85 (time:150′)	8	80 (time:150′)
1 g_{sample}/dm^3, 50 $\mu mol/dm^3$	*Diclofenac*		*Salicylic acid*	
Sample	Adsorption removal (%)	Total elimination (%)	Adsorption removal (%)	Total elimination (%)
Zn_6Al_2	56	93	40	65
$Zn_6Al_{1.5}Ti_{0.5}$	53	91	24	66
Zn_6AlTi	16	58	32	51
$Zn_6Al_{0.5}Ti_{1.5}$	6	0	0	0
Zn_6Ti_2	0	0	0	0
$5Fe/Zn_6Al_2$	93	99	40	53
$5Fe/Zn_6Al_{1.5}Ti_{0.5}$	63	66	30	32
$5Fe/Zn_6AlTi$	63	65	25	32
$5Fe/Zn_6Al_{0.5}Ti_{1.5}$	0	8	5	15
$5Fe/Zn_6Ti_2$	0	5	1	10

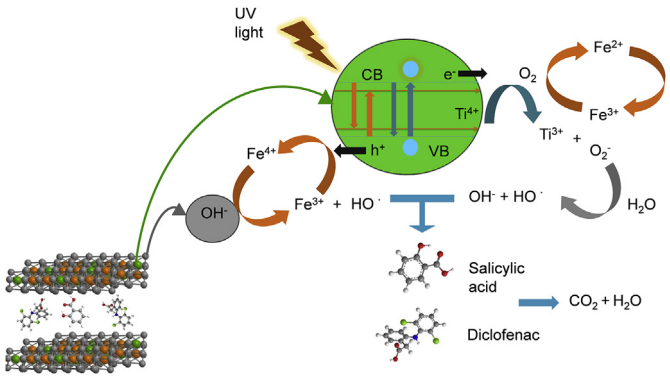

Fig. 8. Schematic diagram showing the mechanism of the photocatalytic reaction taking place on the surface of Fe/ZnAlTi-LDH materials.

$$r = -\frac{dC}{dt} = \frac{k_r K_{ad} C}{1 + K_{ad} C} \qquad \text{Equation (1)}$$

where r is the degradation rate, C the concentration of the organic compound, k_r the intrinsic rate constant and K_{ad} the adsorption equilibrium constant. In the case of a low adsorption and concentration of diclofenac, $K_{ad}C$ can be ignored and r can be expressed as:

$$r = k_r K_{ad} C = K_{app} C \qquad \text{Equation (2)}$$

Setting from the initial conditions ($t = 0$ and $C = C_0$):

$$ln \frac{C_0}{C} = K_{app} t \qquad \text{Equation (3)}$$

The first and second cycles for both samples presented a relevant amount of adsorption, thus making the assumption of Equation (2) impossible and giving poor adjustments to the pseudo-first-order kinetics of Equation (3). However, in the third cycle, adsorption was responsible for less than 10% of the decrease in diclofenac concentration for both samples. As such, the results for cycles 3 and 4 fitted well to pseudo-first-order kinetics. The reaction constant and $t_{1/2}$ for both samples, and the good fit of the results, are shown in Table 6. It can be seen that the K_{app} for 5Ti/$Zn_6Al_{1.33}Fe_{0.66}$ (0.011) is almost twice that of Zn_6Al_2 (0.006).

4. Conclusion

The synthesis of hydrotalcite-type materials with the composition Zn—Al—Ti—Fe in which the aluminum used has been extracted from an industrial waste, namely a saline slag generated during the recycling of aluminum, has been reported. The ZnAl material presents a typical hydrotalcite structure, the crystallinity of which decreases as the amount of Fe or Ti increases due to partial substitution of Al. Thermal treatment at 673 K resulted in the formation of mixed oxides took place, with, ZnO, $ZnFe_2O_4$, Fe_3O_4, Fe_2O_3 and probably $ZnAl_2O_4$ being detected, depending on the composition of the sample. In all cases, the N_2 adsorption isotherms at 77 K were type II, and the BET specific surface areas were between 78 and 199 m^2/g.

The calcinated hydrotalcites with composition ZnAlTi and ZnAlFe have been studied as catalysts and catalyst supports, after impregnation with 5 wt% Fe or Ti, in the photocatalytic degradation of diclofenac and salicylic acid, as examples of emerging contaminants, at 298 K and under UV light. The Fe/ZnAlTi catalysts showed the best catalytic behavior, although it was difficult to distinguish between the fraction removed by adsorption and the fraction photodegraded. To try to solve this problem, consecutive photodegradation cycles, in which the catalyst saturated with the

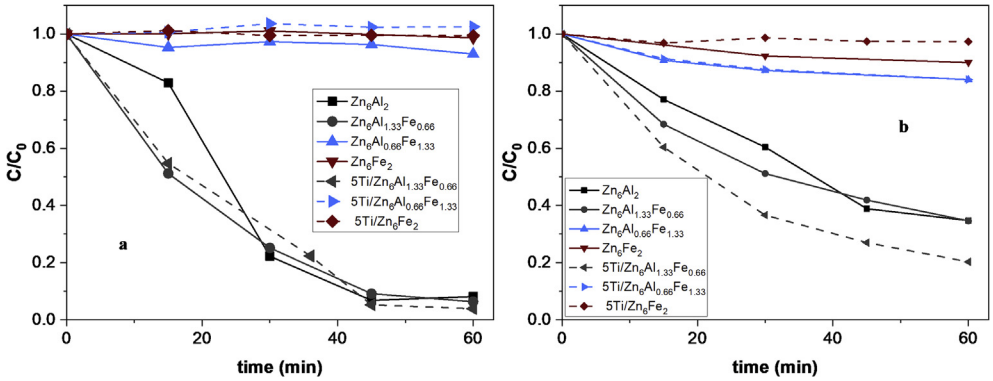

Fig. 9. Comparison of the evolution of the concentration of (a) diclofenac and (b) salicylic acid, with respect to the initial concentration, with irradiation time using ZnAlFe-LDH catalysts. (a,b: 50 $\mu mol_{contaminant}/dm^3$; 1 g_{sample}/dm^3); c: 50 $\mu mol_{contaminant}/dm^3$; 0.3 g_{sample}/dm^3).

Table 5
Diclofenac and salicylic acid removal by adsorption and photodegradation using ZnAlFe-LDH samples as catalysts.

1 g_{sample}/dm^3, 50 $\mu mol/dm^3$	Diclofenac		Salicylic acid	
Sample	Adsorption removal (%)	Total elimination (%)	Adsorption removal (%)	Total elimination (%)
Zn_6Al_2	56	93	40	65
$Zn_6Al_{1.33}Fe_{0.66}$	84	94	59	65
$Zn_6Al_{0.66}Fe_{1.33}$	1	7	16	16
Zn_6Fe_2	1	1	7	10
5Ti/$Zn_6Al_{1.33}Fe_{0.66}$	69	96	49	80
5Ti/$Zn_6Al_{0.66}Fe_{1.33}$	2	0	11	16
5Ti/Zn_6Fe_2	2	1	0	0

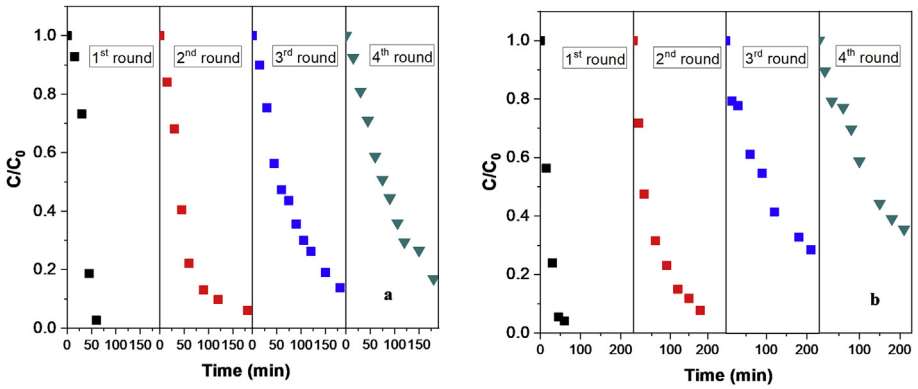

Fig. 10. Comparison of the evolution of the concentration of diclofenac with irradiation time after several cycling runs. (a) $5Ti/Zn_6Al_{1.33}Fe_{0.66}$, (b) Zn_6Al_2 (50 $\mu mol_{contaminant}/dm^3$; 1 g_{sample}/dm^3).

Table 6
Pseudo-first-order kinetic parameters for diclofenac photodegradation.

Catalyst		$t_{1/2}$ (min)	K_{app}
$5Ti/Zn_6Al_{1.33}Fe_{0.66}$	3rd round	56	0.011
	4th round	74	0.010
Zn_6Al_2	3rd round	103	0.006
	4th round	135	0.005

pollutant molecule was used, were performed.

Funding

No funding was received for this work.

CRediT authorship contribution statement

L. Santamaría: Conceptualization, Investigation, Methodology, Supervision, Writing - original draft. **M.A. Vicente:** Conceptualization, Formal analysis, Writing - original draft, Writing - review & editing. **S.A. Korili:** Conceptualization, Supervision, Writing - original draft. **A. Gil:** Conceptualization, Investigation, Formal analysis, Methodology, Supervision, Writing - original draft, Writing - review & editing.

Declaration of competing interest

No conflict of interest exists.

Acknowledgements

This work was funded by the Spanish Ministry of Economy, Industry and Competitiveness (AEI/MINECO), and the European Regional Development Fund (ERDF) through project MAT2016-78863-C2-R and the Government of Navarra through projects PI017-PI039 CORRAL. LS thanks the Universidad Pública de Navarra for a pre-doctoral grant. AG also thanks Banco Santander for funding through the Research Intensification Program.

Appendix A. Supplementary data

Supplementary data to this article can be found online at https://doi.org/10.1016/j.jallcom.2020.156007.

References

[1] T.H. Miller, N.R. Bury, S.F. Owen, J.I. MacRae, L.P. Barron, A review of the pharmaceutical exposome in aquatic fauna, Environ. Pollut. 239 (2018) 129–146, https://doi.org/10.1016/j.envpol.2018.04.012.
[2] V. Pérez-Fernández, L. Mainero Rocca, P. Tomai, S. Fanali, A. Gentili, Recent advancements and future trends in environmental analysis: sample preparation, liquid chromatography and mass spectrometry, Anal. Chim. Acta 983 (2017) 9–41, https://doi.org/10.1016/j.aca.2017.06.029.
[3] K.H. Goh, T.T. Lim, Z. Dong, Application of layered double hydroxides for removal of oxyanions: a review, Water Res. 42 (2008) 1343–1368, https://doi.org/10.1016/j.watres.2007.10.043.
[4] L. Santamaría, M. López-Aizpún, M. García-Padial, M.A. Vicente, S.A. Korili, A. Gil, Zn-Ti-Al layered double hydroxides synthesized from aluminum saline slag wastes as efficient drug adsorbents, Appl. Clay Sci. 187 (2020) 105486, https://doi.org/10.1016/j.clay.2020.105486.
[5] J.S. Valente, F. Tzompantzi, J. Prince, J.G.H. Cortez, R. Gomez, Adsorption and photocatalytic degradation of phenol and 2,4 dichlorophenoxiacetic acid by Mg-Zn-Al layered double hydroxides, Appl. Catal. B Environ. 90 (2009) 330–338, https://doi.org/10.1016/j.apcatb.2009.03.019.
[6] C. Li, M. Wei, D.G. Evans, X. Duan, Layered double hydroxide-based nanomaterials as highly efficient catalysts and adsorbents, Small 10 (2014) 4469–4486, https://doi.org/10.1002/smll.201401464.
[7] S. Nayak, G. Swain, K. Parida, Enhanced photocatalytic activities of RhB degradation and H_2 evolution from in situ formation of the electrostatic heterostructure MoS_2/NiFe LDH nanocomposite through the Z-scheme mechanism via p-n heterojunctions, ACS Appl. Mater. Interfaces 11 (2019) 20923–20942, https://doi.org/10.1021/acsami.9b06511.
[8] S. Nayak, K.M. Parida, Dynamics of charge-transfer behavior in a plasmon-induced quasi-type-II p-n/n-n dual heterojunction in Ag@Ag_3PO_4/g-C_3N_4/NiFe LDH nanocomposites for photocatalytic Cr(VI) reduction and phenol oxidation, ACS Omega 3 (2018) 7324–7343, https://doi.org/10.1021/acsomega.8b00847.
[9] S. Nayak, A.C. Pradhan, K.M. Parida, Topotactic transformation of solvated MgCr-LDH nanosheets to highly efficient porous MgO/$MgCr_2O_4$ nanocomposite for photocatalytic H_2 evolution, Inorg, Inside Chem. 57 (2018) 8646–8661, https://doi.org/10.1021/acs.inorgchem.8b01517.
[10] L. Mohapatra, K. Parida, A review on the recent progress, challenges and perspective of layered double hydroxides as promising photocatalysts, J. Mater. Chem. 4 (2016) 10744–10766, https://doi.org/10.1039/C6TA01668E.
[11] A. Mantilla, F. Tzompantzi, J.L. Fernández, J.A.I.D. Góngora, R. Gómez, Photodegradation of phenol and cresol in aqueous medium by using Zn/Al + Fe mixed oxides obtained from layered double hydroxides materials, Catal, Today Off. 150 (2010) 353–357, https://doi.org/10.1016/j.cattod.2009.11.006.
[12] S.J. Xia, F.X. Liu, Z.M. Ni, J.L. Xue, P.P. Qian, Layered double hydroxides as efficient photocatalysts for visible-light degradation of Rhodamine B, J. Colloid Interface Sci. 405 (2013) 195–200, https://doi.org/10.1016/j.jcis.2013.05.064.
[13] S.J. Xia, F.X. Liu, Z.M. Ni, W. Shi, J.L. Xue, P.P. Qian, Ti-based layered double hydroxides: efficient photocatalysts for azo dyes degradation under visible light, Appl. Catal. B Environ. 144 (2014) 570–579, https://doi.org/10.1016/j.apcatb.2013.07.060.
[14] L.D.L. Miranda, C.R. Bellato, J.L. Milagres, L.G. Moura, A.H. Mounteer, M.F. de Almeida, Hydrotalcite-TiO_2 magnetic iron oxide intercalated with the anionic surfactant dodecylsulfate in the photocatalytic degradation of methylene blue dye, J. Environ. Manag. 156 (2015) 225–235, https://doi.org/10.1016/j.jenvman.2015.03.051.
[15] L. Lambolez, P. Vasseur, J.F. Ferard, T. Gisbert, The environmental risks of industrial waste disposal: an experimental approach including acute and chronic toxicity studies, Ecotoxicol. Environ. Saf. 28 (1994) 317–328, https://doi.org/10.1006/eesa.1994.1056.
[16] G. Power, M. Gräfe, C. Klauber, Bauxite residue issues: I. Current management, disposal and storage practices, Hydrometallurgy 108 (2011) 33–45, https://doi.org/10.1016/j.hydromet.2011.02.006.
[17] L.K. Wang, Y.-T. Hung, N.K. Shammas, Handbook of Advanced Industrial and

Hazardous Wastes Treatment, CRC Press, Taylor & Francis, Boca Raton, 2010.
[18] A. Gil, E. Arrieta, M.A. Vicente, S.A. Korili, Synthesis and CO_2 adsorption properties of hydrotalcite-like compounds prepared from aluminum saline slag wastes, Chem. Eng. J. 334 (2018) 1341–1350, https://doi.org/10.1016/j.cej.2017.11.100.
[19] A. Gil, S. Albeniz, S.A. Korili, Valorization of the saline slags generated during secondary aluminium melting processes as adsorbents for the removal of heavy metal ions from aqueous solutions, Chem. Eng. J. 251 (2014) 43–50, https://doi.org/10.1016/j.cej.2014.04.056.
[20] A. Gil, S.A. Korili, Management and valorization of aluminum saline slags: current status and future trends, Chem. Eng. J. 289 (2016) 74–84, https://doi.org/10.1016/j.cej.2015.12.069.
[21] L. Cocheci, L. Lupa, M. Gheju, A. Golban, R. Lazău, R. Pode, Zn–Al–CO_3 layered double hydroxides prepared from a waste of hot-dip galvanizing process, Clean Technol. Environ. Policy 20 (2018) 1105–1112, https://doi.org/10.1007/s10098-018-1533-3.
[22] R. Galindo, A. López-Delgado, I. Padilla, M. Yates, Hydrotalcite-like compounds: a way to recover a hazardous waste in the aluminium tertiary industry, Appl. Clay Sci. 95 (2014) 41–49, https://doi.org/10.1016/j.clay.2014.03.022.
[23] N. Murayama, J. Shibata, K. Sakai, S. Nakajima, H. Yamamoto, Synthesis of hydrotalcite-like materials from various wastes in aluminum regeneration process, Resour. Process. 53 (2009) 6–11, https://doi.org/10.4144/rpsj.53.6.
[24] Y. Kuwahara, T. Ohmichi, T. Kamegawa, K. Mori, H. Yamashita, A novel conversion process for waste slag: synthesis of a hydrotalcite-like compound and zeolite from blast furnace slag and evaluation of adsorption capacities, J. Mater. Chem. 20 (2010) 5052–5062, https://doi.org/10.1039/C0JM00518E.
[25] N.N. Das, J. Konar, M.K. Mohanta, A.K. Upadhaya, Synthesis, characterization and adsorptive properties of hydrotalcite-like compounds derived from titanium rich bauxite, React. Kinet. Mech. Catal. 99 (2010) 167–176, https://doi.org/10.1007/s11144-009-0120-3.
[26] B. Ferrari, N. Paxéus, R. Lo Giudice, A. Pollio, J. Garric, Ecotoxicological impact of pharmaceuticals found in treated wastewaters: study of carbamazepine, clofibric acid, and diclofenac, Ecotoxicol. Environ. Saf. 55 (2003) 359–370, https://doi.org/10.1016/S0147-6513(02)00082-9.
[27] E. Vulliet, C. Cren-Olivé, M.F. Grenier-Loustalot, Occurrence of pharmaceuticals and hormones in drinking water treated from surface waters, Environ. Chem. Lett. 9 (2011) 103–114, https://doi.org/10.1007/s10311-009-0253-7.
[28] E. Carmona, V. Andreu, Y. Picó, Occurrence of acidic pharmaceuticals and personal care products in Turia River Basin: from waste to drinking water, Sci. Total Environ. 484 (2014) 53–63, https://doi.org/10.1016/j.scitotenv.2017.04.102.
[29] M. Yoldi, E.G. Fuentes-Ordoñez, S.A. Korili, A. Gil, Efficient recovery of aluminum from saline slag wastes, Miner. Eng. 140 (2019) 105884, https://doi.org/10.1016/j.mineng.2019.105884.
[30] M. Shao, J. Han, M. Wei, D.G. Evans, X. Duan, The synthesis of hierarchical Zn-Ti layered double hydroxide for efficient visible-light photocatalysis, Chem. Eng. J. 168 (2011) 519–524, https://doi.org/10.1016/j.cej.2011.01.016.
[31] D. Carriazo, M. del Arco, E. García-López, G. Marci, C. Martín, L. Palmisano, V. Rives, Zn, Al hydrotalcites calcined at different temperatures: preparation, characterization and photocatalytic activity in gas-solid regime, J. Mol. Catal. Chem. 342–343 (2011) 83–90, https://doi.org/10.1016/j.molcata.2011.04.015.
[32] K.M. Parida, N. Ballarsingh, B. Sairam Patra, J. Das, Copperphtalocyanine immobilized Zn/Al LDH as photocatalyst under solar radiation for decolorization of methylene blue, J. Mol. Catal. Chem. 267 (2007) 202–208, https://doi.org/10.1016/j.molcata.2006.11.035.
[33] A.V.F. Cavani, F. Trifiro, Hydrotalcite-type anionic clays: preparation, properties and applications, Catal, Today Off. 11 (1991) 173–301, https://doi.org/10.1016/0920-5861(91)80068-K.
[34] B.D. Cullity, Elements of X-Ray Diffraction, Addison-Wesley Publishing Company, 1978.
[35] R.D. Shannon, Revised effective ionic radii and systematic studies of interatomie distances in halides and chaleogenides, Acta Crystallogr. 32 (1976) 751–767, https://doi.org/10.1107/S0567739476001551.
[36] X. Cheng, X. Huang, X. Wang, D. Sun, Influence of calcination on the adsorption removal of phosphate by Zn-Al layered double hydroxides from excess sludge liquor, J. Hazard Mater. 177 (2010) 515–523, https://doi.org/10.1016/j.jhazmat.2009.12.063.
[37] M.J. dos Reis, V. Prévot, F. Leroux, F. Silvério, J. Barros Valim, Dendrimer intercalation in layered double hydroxides, J. Porous Mater. 17 (2010) 443–451, https://doi.org/10.1007/s10934-009-9306-3.
[38] M. Hadnadjev-Kostic, T. Vulic, R. Marinkovic-Neducin, D. Loncarevic, J. Dostanic, S. Markov, D. Jovanovic, Photo-induced properties of photocatalysts: a study on the modified structural, optical and textural properties of TiO_2-ZnAl layered double hydroxide based materials, J. Clean. Prod. 164 (2017) 1–18, https://doi.org/10.1016/j.jclepro.2017.06.091.
[39] R.J. Balasamy, B.B. Tope, A. Khurshid, A.A.S. Al-Ali, L.A. Atanda, K. Sagata, M. Asamoto, H. Yahiro, K. Nomura, T. Sano, K. Takehira, S.S. Al-Khattaf, Ethylbenezene dehydrogenation over FeO_x/(Mg,Zn)(Al)O catalysts derived from hydrotalcites: role of MgO as basic sites, Appl. Catal. Gen. 398 (2011) 113–122.
[40] M.R. Mohammadi, D.J. Fray, Low temperature nanostructured zinc titanate by an aqueous particulate sol-gel route: optimisation of heat treatment condition based on Zn:Ti molar ratio, J. Eur. Chem. Soc. 30 (2010) 947–961, https://doi.org/10.1016/j.jeurceramsoc.2009.09.031.
[41] A. Lak, A. Simchi, Z. Ali Nemati, Photocatalytic activity of TiO_2-capped ZnO nanoparticles, J. Mater. Sci. Mater. Electron. 23 (2012) 361–369, https://doi.org/10.1007/s10854-011-0396-8.
[42] O. Saber, T. Zaki, Carbon monoxide oxidation using Zn-Cu-Ti hydrotalcite-derived catalysts, J. Chem. Sci. 126 (2014) 981–988, https://doi.org/10.1007/s12039-014-0642-8.
[43] K. Horni, O. Abdelkarim, N. Frini-Srasra, E. Srasra, Synthesis, structure and photocatalytic activity of calcined Mg-Al-Ti-layered double hydroxides, Kor. J. Chem. Eng. 32 (2015) 104–112, https://doi.org/10.1007/s1814-014-0199-8.
[44] E.M. Seftel, M.C. Puscasu, M. Mertens, P. Cool, G. Carja, Assemblies of nanoparticles of CeO_2-ZnTi-LDHs and their derived mixed oxides as novel photocatalytic systems for phenol degradation, Appl. Catal. B Environ. 150–151 (2014) 157–166, https://doi.org/10.1016/j.apcatb.2013.12.019.
[45] L. Fang, W. Li, H. Chen, F. Xiao, L. Huang, P.E. Holm, H.ChB. Hansen, D. Wang, Synergistic effect of humic and fulvic acids on Ni removal by the calcined Mg/Al layered double hydroxide, RSC Adv. 5 (2015) 18866–18874, https://doi.org/10.1039/C4RA15406A.
[46] G. Chen, S. Qian, X. Tu, X. Wei, J. Zou, L. Leng, S. Luo, Enhancement photocatalytic degradation of rhodamine B on nanoPt intercalated Zn-Ti layered double hydroxides, Appl. Surf. Sci. 293 (2014) 345–351, https://doi.org/10.1016/j.apsusc.2013.12.165.
[47] P. Benito, I. Guinea, F.M. Labajos, J. Rocha, V. Rives, Microwave-hydrothermally aged Zn,Al hydrotalcite-like compounds: influence of the composition and the irradiation conditions, Microporous Mesoporous Mater. 110 (2008) 292–302, https://doi.org/10.1016/j.micromeso.2007.06.013.
[48] P.A. Webb, C. Orr, Analytical Methods in Fine Particle Technology, Micromeritics Instrument Corporation, 1997.
[49] M. Liang, W. Kang, K. Xie, Comparison of reduction behavior of Fe_2O_3, ZnO and $ZnFe_2O_4$ by TPR technique, J. Nat. Gas Chem. 18 (2009) 110–113, https://doi.org/10.1016/S1003-9953(08)60073-0.
[50] P. Naknam, A. Luengnaruemitchai, S. Wongkasemjit, Au/ZnO and Au/ZnO–Fe_2O_3 prepared by deposition–precipitation and their activity in the preferential oxidation of CO, Energy Fuels 23 (2009) 5084–5091, https://doi.org/10.1021/ef9004187.
[51] E.M. Fuentes, A.C.F. Junior, T.F. Silva, J.M. Assaf, M.C. Rangel, A comparison between copper and nickel-based catalysts obtained from hydrotalcite-like precursors for WGSR, Catal. Today 171 (2011) 290–296, https://doi.org/10.1016/j.cattod.2011.03.082.
[52] A. Khan, P.G. Smirniotis, Relationship between temperature-programmed reduction profile and activity of modified ferrite-based catalysts for WGS reaction, J. Mol. Catal. Chem. 280 (2008) 43–51, https://doi.org/10.1016/j.molcata.2007.10.022.
[53] L. Santamaría, M.A. Vicente, S.A. Korili, A. Gil, Effect of the preparation method and metal content on the synthesis of metal modified titanium oxide used for the removal of salicylic acid under UV light, Environ. Technol. 41 (2020) 2073–2084, https://doi.org/10.1080/09593330.2018.1555285.
[54] E. McCafferty, J.P. Wightmam, Determination of the concentration of Surface hydroxyl groups on metal oxide films by a quantitative XPS method, Surf. Interface Anal. 26 (1998) 549–564, https://doi.org/10.1002/(sici)1096-9918(199807)26:8<549:aid-sia396>3.0.co;2-q.
[55] A. Mantilla, G. Jácome-Acatitla, G. Morales-Mendoza, F. Tzompantzi, R. Gomez, Photoassisted degradation of 4-chlorophenol and p-cresol using MgAl hydrotalcites, Ind. Eng. Chem. Res. 50 (2011) 2762–2767, https://doi.org/10.1021/ie1006883.
[56] L. Mohapatra, K. Parida, M. Satpathy, Molybdate/tungstate intercalated oxo-bridged Zn/Y LDH for solar light induced photodegradation of organic pollutants, J. Phys. Chem. C 116 (2012) 13063–13070, https://doi.org/10.1021/jp300066g.